Investigations on the chip formation mechanism and shear localization sensitivity of high-speed machining Ti6Al4V

Bing Wang & Zhanqiang Liu

The International Journal of Advanced Manufacturing Technology

ISSN 0268-3768
Volume 75
Combined 5-8

Int J Adv Manuf Technol (2014)
75:1065-1076
DOI 10.1007/s00170-014-6191-y

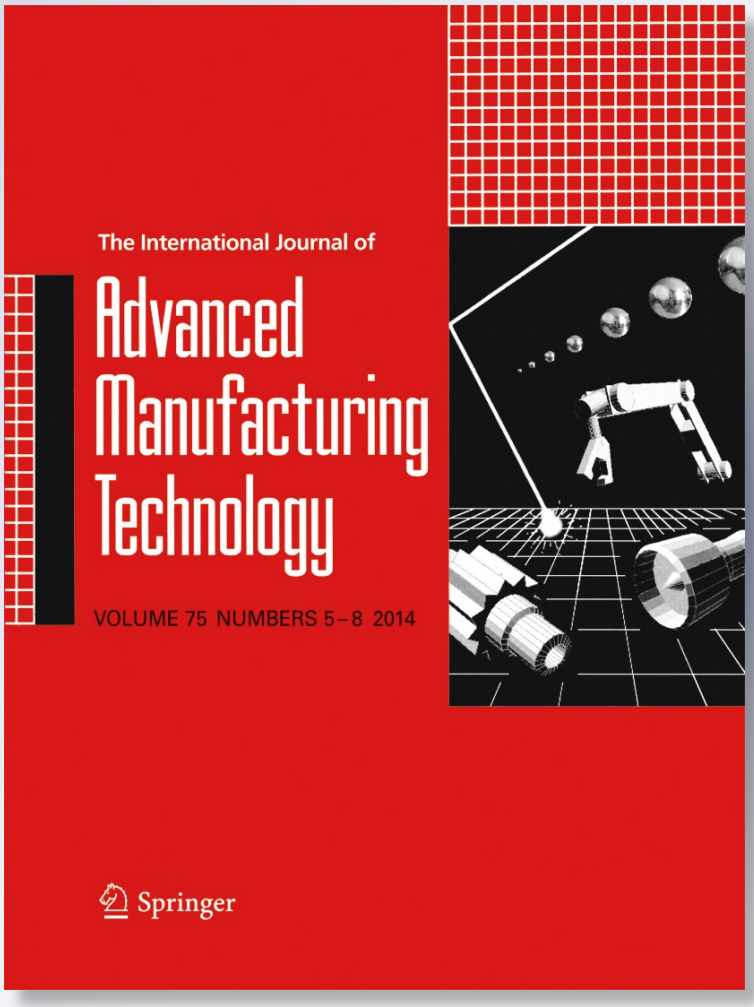

Springer

Int J Adv Manuf Technol (2014) 75:1065–1076
DOI 10.1007/s00170-014-6191-y

ORIGINAL ARTICLE

Investigations on the chip formation mechanism and shear localization sensitivity of high-speed machining Ti6Al4V

Bing Wang · Zhanqiang Liu

Received: 18 February 2014 / Accepted: 21 July 2014 / Published online: 10 August 2014

Abstract This study develops a combined numerical and experimental approach to get deeper insights into chip formation mechanism for high-speed machining of titanium alloy Ti6Al4V. The numerical investigation of high-speed machining is implemented with the aid of finite element analysis software Abaqus/Explicit, in which the Johnson-Cook (JC) fracture model with an energy-based ductile failure criterion is adopted. Meanwhile, the experiments of high-speed orthogonal cutting are carried out to validate the numerical results. The cutting speeds are selected ranging from 50 to 3,000 m/min, and the uncut chip thickness is fixed at 0.1 mm. The variables investigated include the serrated degree and serrated frequency of chips in addition to the cutting force. The results show that both the serrated degree and serrated frequency have positive correlations with the cutting speed. An important regularity for the transformation of chip morphology from serrated to unit at a critical cutting speed has been achieved, and the critical value for Ti6Al4V is about 2,500 m/min. The research also finds that the cutting force decreases with the increasing cutting speed, while its fluctuant frequency and amplitude increase sharply. Furthermore, the influences of JC fracture constants (the five constants in JC fracture model) on chip formation are investigated based on the finite element method, which is the main original and innovative highlight of this study. The shear localization sensitivity is firstly proposed to describe the influences of JC fracture constants on the chip formation process. When the JC fracture constants decrease, the shear localization sensitivity is positive which means that the serrated degree increases and vice versa. The sensitivity analyses indicate that the influences of initial failure strain D_1 and exponential factor of stress triaxiality D_2 on chip formation process are more conspicuous than the rest three ones. This paper is enticing from both the engineering and the analytical perspectives aimed at predicting the evolution of serrated chip formation and chip morphology transformation in metal cutting process.

Keywords Finite element method · JC fracture model · Shear localization sensitivity · High-speed machining · Ti6Al4V

Nomenclature

A	Initial yield stress (MPa)
a_c	Uncut chip thickness (mm)
B	Hardening modulus (MPa)
C	Strain rate dependency coefficient
d	Pitch of two neighboring trapezoids in serrated chips (mm)
D	Damage variable
d_1	Diameter of slot milling cutter (mm)
d_2	Width of workpiece (mm)
D_1	Initial failure strain of JC fracture model
D_2	Exponential factor of JC fracture model
D_3	Triaxiality factor of JC fracture model
D_4	Strain rate factor of JC fracture model
D_5	Temperature factor of JC fracture model
f	Chip serrated frequency

B. Wang · Z. Liu
School of Mechanical Engineering, Shandong University, Jinan, Shandong 250061, People's Republic of China

B. Wang · Z. Liu (✉)
Key Laboratory of High Efficiency and Clean Mechanical Manufacture, Shandong University, Ministry of Education, Jinan, Shandong, People's Republic of China
e-mail: melius@sdu.edu.cn

G_f	Fracture energy required to form a unit area of crack (J)
G_s	Chip serrated degree
$G_s^{D_i}$	Chip serrated degree under different fracture constants
G_s^{original}	Chip serrated degree under the original fracture constants
h	Discontinuous section height of serrated chip (mm)
H	Maximum height of serrated chip (mm)
L	Characteristic length to determine the stress-displacement response (mm)
m	Thermal softening coefficient
n	Strain hardening coefficient
P	Average of three normal stresses, also called the hydrostatic pressure (MPa)
S	Shear localization sensitivity of serrated chip
T	Temperature at a given calculation instant (K)
T_m	Melting temperature of workpiece material (K)
T_r	Room temperature (K)
$\overline{u}$	Equivalent plastic displacement (mm)
$\overline{u}_f$	Equivalent plastic displacement at fracture (mm)
V	Cutting speed (m/min)
w	Damage initiation parameter
$\overline{\varepsilon}$	Equivalent plastic strain
$\overline{\varepsilon}_0$	Initial plastic strain
$\dot{\overline{\varepsilon}}$	Equivalent strain rate (s^{-1})
$\dot{\overline{\varepsilon}}_0$	Reference strain rate (s^{-1})
$\overline{\varepsilon}_f$	Equivalent strain at fracture
$\Delta\overline{\varepsilon}$	Increment of equivalent plastic strain
$\overline{\sigma}$	Equivalent stress (MPa)
σ_y	Yield stress (MPa)

1 Introduction

Titanium alloys have excellent properties such as high specific strength (strength-to-weight ratio), high toughness, high temperature resistance, corrosion resistance, etc. These admirable properties make titanium alloys bear high load and maintain sufficient strength at elevated temperature [1–3]. Therefore, the titanium alloys have been applied in the automotive and aerospace industries, medical equipments and implants, chemical processing components, power stations, nuclear and marine applications, etc. [4]. As the same as other materials, titanium alloys should be subjected to manufacturing operations before entering into service. The machining process is one of the most important manufacturing processes due to the superior surface quality added to the finished products. Most mechanical components made from titanium alloys are still fabricated by conventional machining processes such as turning, milling, drilling, grinding, boring, and reaming.

However, the utilization of titanium alloys is restricted by their poor machinability. Hitherto, many researchers have paid attention to the investigations on machining mechanism of titanium alloys, which includes chip formation mechanism [5], cutting force and cutting temperature [6], finished surface quality [7], tool wear and tool failure [8], etc. Due to the unique properties of titanium alloys, especially for their poor thermal property, the chips produced are serrated even when the cutting speed is very low, which is distinctly different from other materials. As the chip formation has great effect on the variation of cutting force, the distribution of cutting temperature in addition to the tool wear and tool failure, it is important to have deeper insights into the essential factors which control the chip formation mechanism. Many researches have paid attention to the formation mechanism of serrated chips, which can mainly be summarized as adiabatic shear theory [9–11] and periodic crack theory [12–14]. The chip formation is dominated by the material properties and mechanical conditions during the cutting process, in which the material undergoes severe deformation within the primary shear zone. However, the dynamic mechanical behavior of materials under the coupling influences of large strains, high strain rates, and elevated temperatures is still poorly understood, and the relevant theoretical analyses are difficult to proceed. It is more convenient and feasible to analyze the material behavior during chip formation process based on finite element method.

Previously, several different numerical methods were used to simulate serrated chip formation. These methods were based on either implicit or explicit software packages such as Deform [15], Ansys [16], Abaqus [17], Forge [18], Advantedge™ [19], SPH [20], etc. Various models have been developed involving different meshes, plasticity models, and fracture models, which mainly include strain-based fracture criterion, the Johnson-Cook (JC) fracture model, the Cockcroft-Latham fracture criterion, and without fracture criterion [21–24]. To accurately conduct the research of cutting process based on finite element method, the reasonable selection of material constitutive model under severe loading conditions is prerequisite and of vital importance. In addition, the success and reliability of numerical analyses are heavily dependent on the material flow stress, the friction parameters between the tool–chip interface, the mechanical and thermal parameters, and the material separation criterion [25, 26]. In consideration of the mechanical characteristics and deformation status during metal cutting process, the JC constitutive model and JC fracture model are most widely used, which take the coupling effects of strain, strain rate, and temperature into account. Recently, cutting simulations have been performed more precisely and realistically by incorporating progressive failure model with chip separation criterion or adaptive meshing method into the finite element analyses [27, 28]. The most important factor in the progressive failure model is

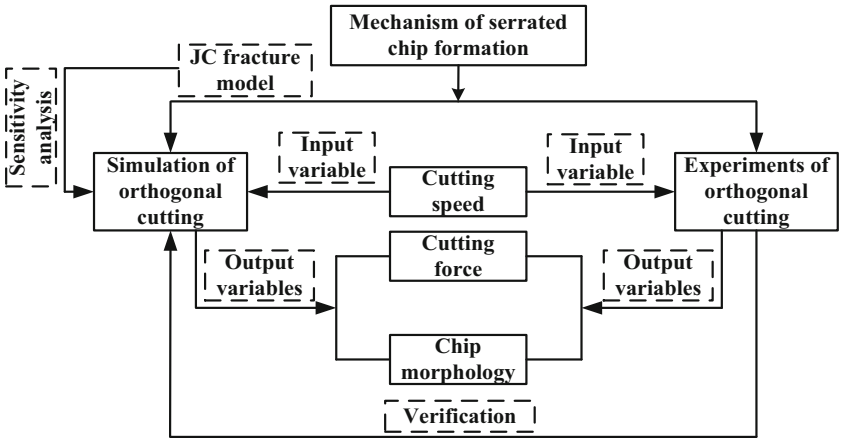

Fig. 1 Outline of this study

to properly implant the damage evolution criterion into the failure model. There are two ways applied to determine the damage evolution in Abaqus software which are defined as the equivalent plastic displacement and fracture energy dissipation. Ambati and Yuan [29] researched the mesh dependence in cutting simulation based on the plastic displacement damage evolution criterion with exponential softening. Their results demonstrate that the effect of element size on computational results is reduced significantly if the failure criterion in the process simulation is controlled by a characteristic element length considered from the progressive damage model. Umbrello [30] conducted the finite element analyses of cutting force, chip morphology, and segmentation during conventional and high-speed machining Ti6Al4V, in which three JC constitutive equations with different sets of material constants were implemented. The results indicate that a good prediction of both principal cutting force and chip morphology can be achieved only if the material constants for the JC constitutive equation adopted are reasonable. Hosseini and Kazeminezhad [31] proposed a new and better constitutive model in finite element method to investigate the material behavior during intense deformation. The model is completely based on physical mechanism that can predict all stages of flow stress evolution and also can elucidate the effects of strain and strain rate on flow stress evolution of material during intense plastic deformation which can be used in the simulation of high-speed machining. There are also other scholars who have investigated the metal cutting process with the aid of finite element method in such aspects as chip morphology [32, 33], burr formation [34], orthogonal micro-machining process [20], etc.

There has been a considerable amount of research to study the serrated chip formation mechanism of titanium alloys depending on the finite element simulation of machining, in which different material failure models have also been implanted. Nevertheless, the influences of different material fracture models, especially the influences of fracture model parameters, have not yet been understood completely. Because the material fracture process involves the roles of strain, strain rate, and temperature, it is also important to investigate the different influences of these three variables. Research of the influences of fracture model parameters on the chip formation process can help to understand the essence of chip deformation or fracture under different cutting parameters.

The main objective of this paper concerns the presentation of numerical and experimental analyses for orthogonal cutting process in order to get deeper insights into the mechanism of serrated chip formation. Figure 1 illustrates the outline of the research. One aim of this research is to conduct the comparison between the numerical and the experimental results with respect to the cutting force and chip morphology under different cutting conditions, which can validate the reliability of the numerical analyses. Then, the chip morphology and serrated degree are analyzed through the finite element simulation with different JC fracture constants. In addition, the concept of shear localization sensitivity is proposed to investigate the influences of JC fracture constants on the chip formation process. This novel concept can help to evaluate the influences of JC fracture constants on the chip formation quantitatively. Consequently, the control mechanism of material property on the chip formation is further revealed. Among all

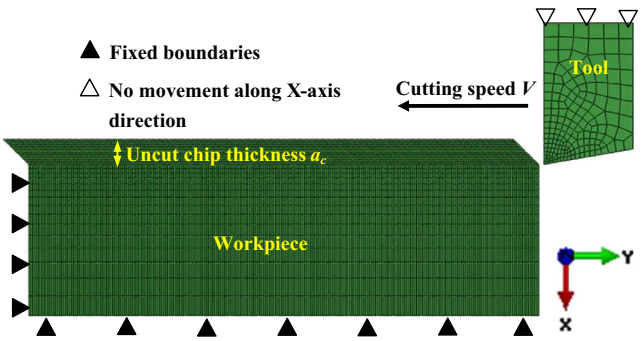

Fig. 2 Schematic of finite element model for orthogonal cutting

Table 1 JC constitutive model parameters of Ti6Al4V [37]

A (MPa)	*B* (MPa)	*n*	*C*	*m*
862	331	0.34	0.012	0.8

titanium alloys, Ti6Al4V is the most widely used and so it has been chosen as the workpiece material in this research.

2 Finite element method and modeling procedure

The finite element analysis software Abaqus/Explicit was adopted to simulate the two-dimensional orthogonal cutting process of Ti6Al4V. The process of serrated chip formation was analyzed after modeling the tool, workpiece, relevant properties of materials, contact, and boundary conditions. Through analyses of cutting process under different fracture model parameters, the shear localization sensitivity of serrated chips to fracture model parameters in machining Ti6Al4V is deduced, which can help to improve the comprehension of serrated chip formation mechanism.

2.1 Modeling of orthogonal cutting

The numerical method developed with Abaqus/Explicit was adopted because it can avoid the convergence caused by the contact and material complexities [35]. The finite element model was established by using the planar quadrilateral continuum elements (CPE4RT) which are suitable for the coupled temperature-displacement calculation and have reduced integration and hourglass control features. An element deletion technique was used to allow element separation to form chip. Once the nodes in element reach the degradation value of 1, it is separated and excluded from the computation. Cutting tool is constrained as a rigid body and its rake angle is 0°. The cutting speeds V are set from 50 to 3,000 m/min which are parallel to the workpiece as shown in Fig. 2. Workpiece is fixed in bottom and left sides against both vertical and horizontal movements. The uncut chip thickness a_c is set at 0.1 mm which is kept constant for all simulations. Contact definition between cutting tool and workpiece is defined by using penalty contact model, in which the tool surface is the master one while the chip face is the slave one. So, the mesh density of the chip layer is larger than that of the tool. The chip–tool friction is based on Coulomb's friction law which is used in many previous researches [17, 32]. A chamfer is designed on the removed material layer to avoid distortion problems at the beginning of calculation.

2.2 Constitutive model of Ti6Al4V

In finite element method, accurate material flow stress models are highly essential to describe the workpiece material behavior under high strain rate deformation conditions. The JC constitutive model is considered the most widely in the simulation of high-speed machining because it is a thermal viscoplastic model suitable for conditions where the strain rate is over a large range from 10^2 to 10^6 s^{-1} [36]. The effects of strain hardening, strain rate hardening, and thermal softening are taken into account simultaneously. The JC constitutive model is expressed by Eq. (1).

$$\bar{\sigma} = \underbrace{\left[A + B\bar{\varepsilon}^{n}\right]}_{\text{Elastoplastic term}} \underbrace{\left[1 + C\ln\left(\frac{\dot{\bar{\varepsilon}}}{\dot{\bar{\varepsilon}}_0}\right)\right]}_{\text{Viscosity term}} \underbrace{\left[1-\left(\frac{T-T_r}{T_m-T_r}\right)^{m}\right]}_{\text{Thermal softening term}} \tag{1}$$

where $\bar{\sigma}$ is the equivalent stress, $\bar{\varepsilon}$ is the equivalent plastic strain, $\dot{\bar{\varepsilon}}$ is the equivalent strain rate, $\dot{\bar{\varepsilon}}_0$ is the reference strain rate. The parameters T, T_m, and T_r are current temperature, melting temperature of workpiece material, and room temperature, respectively. A is the initial yield stress, B is the hardening modulus, n is the strain hardening coefficient, C is the strain rate dependency coefficient, and m is the thermal softening coefficient. The JC constitutive model parameters and the physical and mechanical properties of Ti6Al4V used to simulate its mechanical behavior are specified in Tables 1 and 2, respectively.

The tools used in the simulations are tungsten carbide inserts whose rake angle and flank angle are 0° and 10°, respectively. The physical parameters of cutting tools are presented in Table 3.

2.3 Chip separation criterion

In order to simulate the emergence of chip formation, a fracture model that gives rise to chip detachment is used.

Table 2 Physical and mechanical properties of Ti6Al4V [24]

Density (kg/m^3)	Elastic modulus (GPa)	Poisson's ratio	Thermal conductivity (W/m K)	Specific heat (J/kg K)	Thermal expansion coefficient (/K)	Melting temperature (K)
4,430	109 (323 K) 91 (523 K) 75 (723 K)	0.34	6.8 (293 K) 7.4 (373 K) 9.8 (573 K) 11.8 (773 K)	611 (293 K) 624 (373 K) 674 (573 K) 703 (773 K)	9.0E-6	1,878

Table 3 Physical parameters of the tungsten carbide cutting tools [32]

Density (kg/m^3)	Elastic modulus (GPa)	Poisson's ratio	Thermal conductivity (W/m K)	Specific heat (J/kg K)
11,900	534	0.22	50	400

The fracture model is established according to the classical cumulative damage law expressed by Eq. (2), in which the JC fracture model [38] has been developed.

$$w = \sum \frac{\Delta\bar{\varepsilon}}{\bar{\varepsilon}_f} \tag{2}$$

where $\Delta\bar{\varepsilon}$ is the increment of equivalent plastic strain which occurs during an integration cycle and $\bar{\varepsilon}_f$ is the equivalent strain to fracture under the current conditions of strain rate, temperature, pressure, and equivalent stress. Damage is then allowed to initiate when w=1.0. The general expression for the JC fracture strain is shown as Eq. (3) [38].

$$\bar{\varepsilon}_f = \left[D_1 + D_2 \exp\left(D_3 \frac{P}{\bar{\sigma}}\right)\right]\left[1 + D_4 \ln\frac{\dot{\bar{\varepsilon}}}{\dot{\bar{\varepsilon}}_0}\right]\left[1 + D_5 \frac{T - T_r}{T_m - T_r}\right] \tag{3}$$

where P is the average of three normal stresses and it is also called the hydrostatic pressure. The ratio of $\frac{P}{\bar{\sigma}}$ is referred to as the stress triaxiality. It can be seen from Eq. (3) that the fracture strain $\bar{\varepsilon}_f$ depends on the stress triaxiality, the equivalent strain rate, the temperature, as well as the fracture constants D_i (i=1, 2, 3, 4, 5). The five fracture constants indicate initial failure strain, exponential factor, triaxiality factor, strain rate factor, and temperature factor, respectively. The fracture constants of JC fracture model for Ti6Al4V are presented in Table 4. One main object of this paper is to investigate the influences of JC fracture constants on the chip formation during high-speed machining Ti6Al4V through the simulation with different JC fracture constants. Then, the effects of shear localization sensitivity of serrated chips to JC fracture constants can be deduced.

In this study, an energy-based ductile failure criterion is applied to illustrate the material behavior of damage evolution during high-speed machining [39]. This model defines the fracture energy G_f as a material parameter which denotes the energy required to form a unit area of crack. The parameter G_f is also called Hillerborg's fracture energy. It governs the weakening of workpiece material according to a stress-displacement response after damage initiation rather than a stress–strain response, so it is favorable to reduce the mesh dependency. Hillerborg's fracture energy can be expressed as Eq. (4).

$$G_f = \int_{\bar{\varepsilon}_0}^{\bar{\varepsilon}_f} L\sigma_y d\bar{\varepsilon} = \int_0^{\bar{u}_f} \sigma_y d\bar{u} \tag{4}$$

where $\bar{\varepsilon}_0$ is the initial plastic strain which is equal to zero before the damage initiates, and L is the characteristic length. The parameter $\bar{u}$ is the equivalent plastic displacement as the fracture work conjugate of the yield stress after onset of the damage. The parameter $\bar{u}_f$ is the equivalent plastic displacement when the fracture occurs. A linear evolution of the damage is assumed, which means that $\bar{u} = L\bar{\varepsilon}$ after the damage initiation. The damage variable D can be expressed by Eq. (5).

$$D = \frac{L\bar{\varepsilon}}{\bar{u}_f} = \frac{\bar{u}}{\bar{u}_f} \tag{5}$$

When the damage variable D reaches 1, the material stiffness is fully degraded, then the relevant elements are deleted and the crack generates.

Figure 3 presents the stress–strain behavior of material undergoing damage evolution [35]. The solid curve OABC

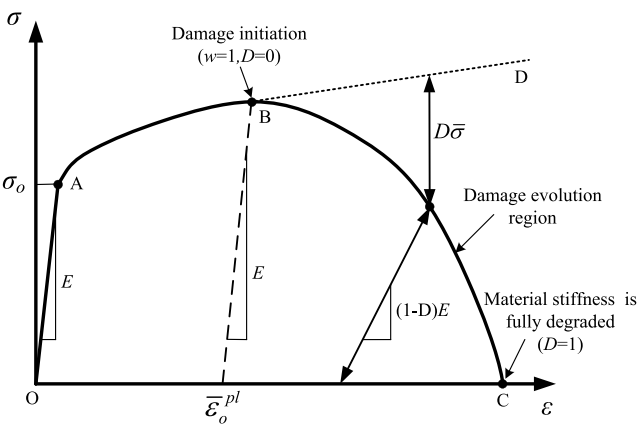

Fig. 3 Stress–strain response of material damage evolution

Table 4 The fracture constants of JC fracture model for Ti6Al4V [37]

D_1	D_2	D_3	D_4	D_5
−0.09	0.25	−0.5	0.014	3.87

illustrates the damaged stress–strain response, while the dashed curve OABD illustrates the stress–strain response assuming there is no damage occurring. The material deformation and fracture process can be divided into three stages as shown in Fig. 3. The first stage OA indicates the linear elastic deformation period. When the stress exceeds the yield stress σ_0, the material enters the second stage AB, in which material undergoes the stable plastic deformation. The effect of strain hardening is prominent in this period. When the cumulative damage parameter w reaches 1 as the point B shows, the plastic instability initiates which turns on the third stage BC. Afterwards, material enters the stage of failure evolution and the thermal softening takes the priority which results in the decrease of the equivalent stress. When the stress–strain curve extends to point C (i.e., the damage variable D reaches 1), the material stiffness is fully degraded and the crack emerges.

3 Comparison of numerical and experimental results

3.1 Experimental setup of orthogonal cutting

Figure 4 shows the schematic and actual photos of experimental setup for orthogonal cutting. The cutting experiments were conducted on Daewoo ACE-V500 vertical machining center whose spindle rotational speed ranges from 80 to 10,000 r/min. The cutter used in the experiments is Kennametal 4.96164-210 90° SN slot milling cutter whose diameter d_1 is 160 mm. The width of workpiece d_2 is 20 mm as shown in Fig. 4. Because the cutter diameter d_1 is much larger than the workpiece width d_2, the directions of cutting force and thrust force can be regarded as approximately parallel with the coordinate axes Y and X, respectively. The insert type is SNHX12L5PZTNGP with coated carbide (KC725M) and its rake angle is 0°. The workpieces were machined at the cutting speeds ranging from 50 to 3,000 m/min, and the feed rate per tooth was fixed at 0.1 mm/z. The feed rate per tooth corresponds to the uncut chip thickness in orthogonal cutting. After each cutting experiment was finished, the insert was replaced by a new one so as to eliminate the influence of tool wear on the experimental results. The axial cutting width is 2.0 mm and the cutting condition is dry cutting. The cutting force was measured by Kistler three-dimensional dynamometer, which was mounted through special fixture on the worktable.

Chips collected after all cutting experiments were inlaid into mosaic materials as specimens, after which the procedures of grinding, polishing, and etching were carried out sequentially. Then, the micrographs of the chips were observed with the aid of VHX-600 ESO digital microscope, by which the relevant geometrical values of chips can be measured.

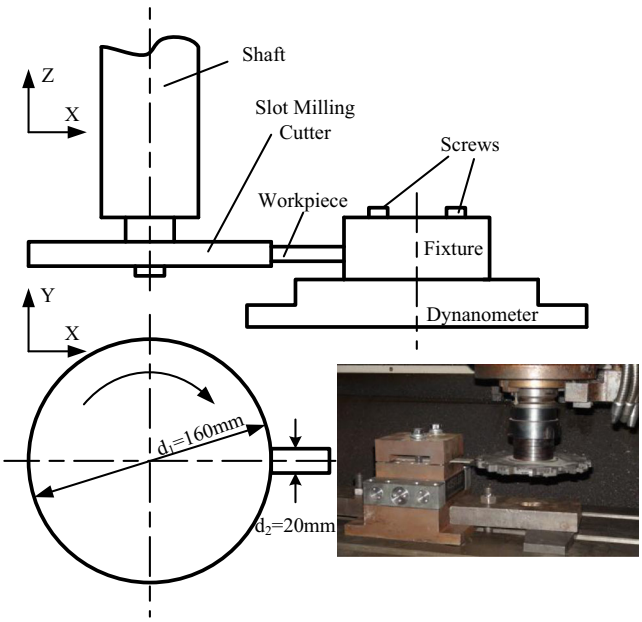

Fig. 4 Experimental setup for orthogonal cutting

3.2 Geometric characteristics of serrated chips

The serrated chip formation can be presented by Fig. 5 in a visualized way. The shadow areas refer to three cutting shear zones as primary shear zone, secondary shear zone, and tertiary shear zone. The geometric characteristics of serrated chips are described by the two parameters of serrated degree G_s and serrated frequency f, which are expressed by Eqs. (6) [40] and (7) [41], respectively. The serrated chip can be regarded as a sequence of trapezoids arranged periodically, and each trapezoid is formed by two shearing planes. If the pitch of two neighboring trapezoids and the chip sliding velocity are known, the serrated frequency can be deduced by Eq. (7).

$$G_s = \frac{h}{H} \tag{6}$$

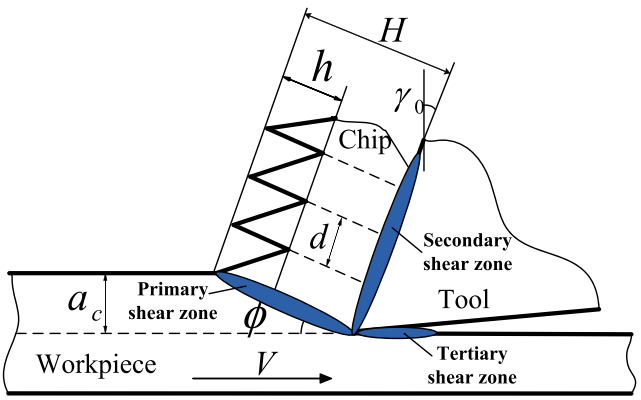

Fig. 5 Schematic of serrated chip formation in orthogonal cutting

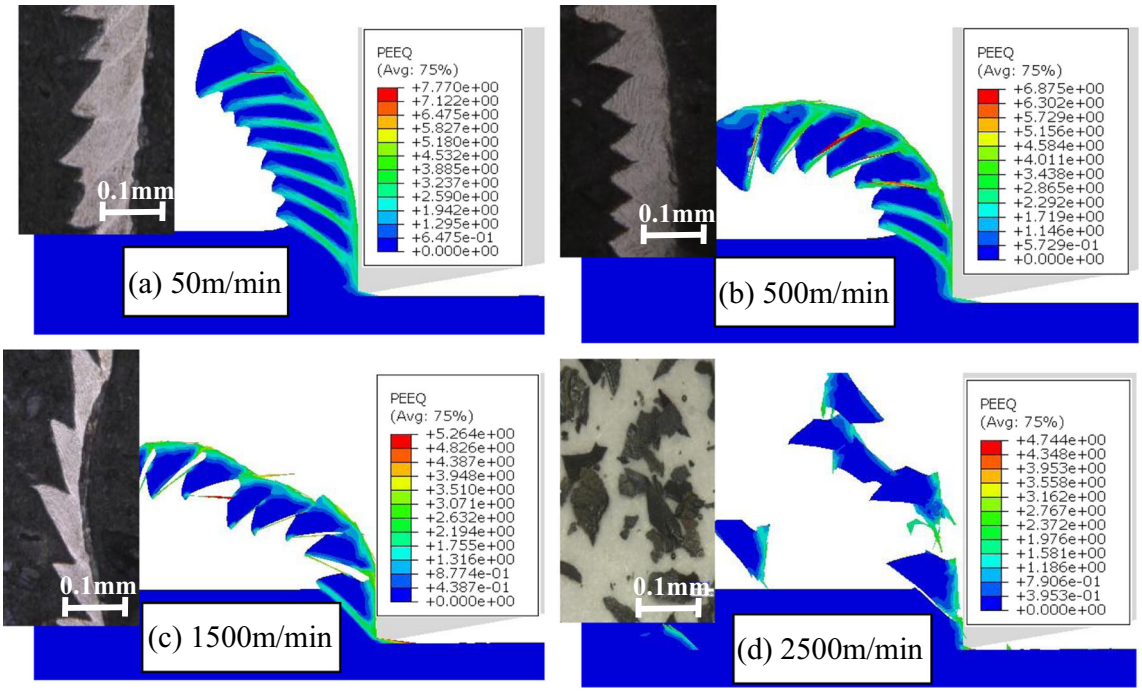

Fig. 6 Variation of chip morphologies under different cutting speeds

where h is the discontinuous section height (i.e., the vertical distance between the valley and the peak of the serrated section) of serrated chip, and H is the maximum height of the serrated chip as shown in Fig. 5.

$$f = \frac{V a_c}{d(H - h/2)} \tag{7}$$

where d is the pitch of two neighboring trapezoids as shown in Fig. 5.

The evolution of chip morphologies with cutting speeds ranging from 50 to 2,500 m/min is presented in Fig. 6, in which the distributions of equivalent plastic strain (PEEQ) can also be seen. As the cutting speed increases, the chip serration is enhanced obviously until the chip morphology evolving to unit at the cutting speed of 2,500 m/min. In the cutting experiments of Ti6Al4V conducted by Sutter and List [5] based on a specific ballistic setup, a chip morphology transition from serrated, more or less regular with localized shearing and possible presence of cracking, to discontinuous at very high speed is also observed. Their results show that the transition speed is 2,700 m/min at the uncut chip thickness of 0.1 mm, which coincides with our results of 2,500 m/min approximately. It can be seen from Fig. 6 that the PEEQ along the primary shear zone and the tool–chip interface (i.e., the secondary shear zone) is larger than that in other areas because the material undergoes severe shear localization in these two positions. Another attractive phenomenon is that the strain in shear zones of serrated chip decreases with the cutting speed increasing. It can be seen that the highest strain in the PEEQ distributions decreases from 7.770 to 4.744 when the cutting speed increases from 50 to 2,500 m/min. The mechanism to govern this result is that the material property changes from plastic to brittle under higher cutting speed, which has been reported in our previous publications [42]. This mechanism can also explain why the chip evolves from continuous to serrated until it is fractured completely.

Figure 7 shows that the variation of chip serrated degree G_s under different cutting speeds based on Eq. (6). The serrated degree G_s has positive correlation with the cutting speed. When the cutting speed reaches 2,500 m/min, the parameter G_s tends to 1, which means that the adjacent segmentations of serrated chips are separated completely as shown in Fig. 6.

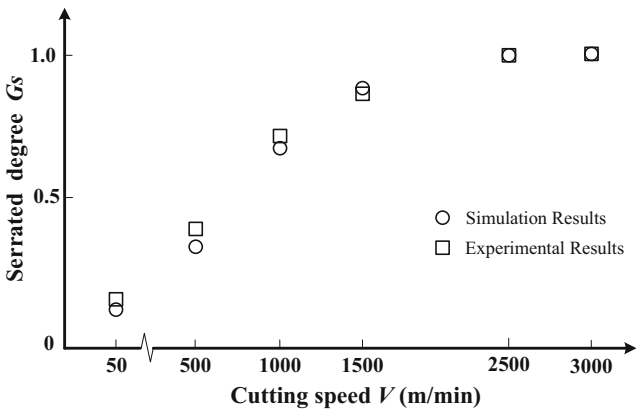

Fig. 7 Variation of serrated degree under different cutting speeds

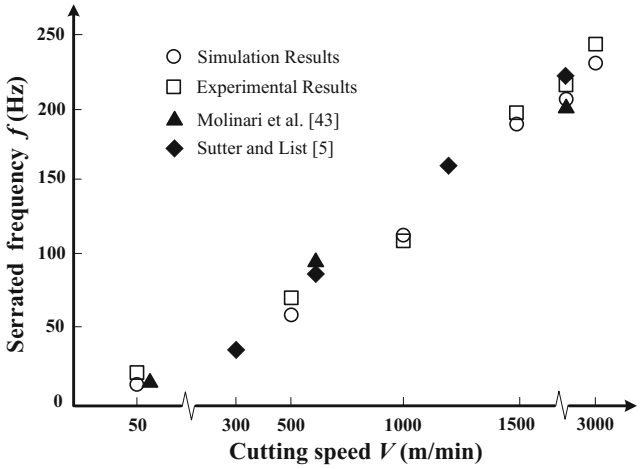

Fig. 8 Variation of serrated frequency under different cutting speeds [5, 43]

The variation of chip serrated frequency f under different cutting speeds based on Eq. (7) is illustrated in Fig. 8. It can be seen that the parameter f increases obviously with the cutting speed increasing. The magnitude of serrated frequency f in this study matches well with the results obtained by Molinari et al. [43] and Sutter and List [5] as shown in Fig. 8. When the serrated chip evolves to unit ones at the cutting speed of 2,500 m/min, the parameter f could not be used to describe the chip geometric characteristics.

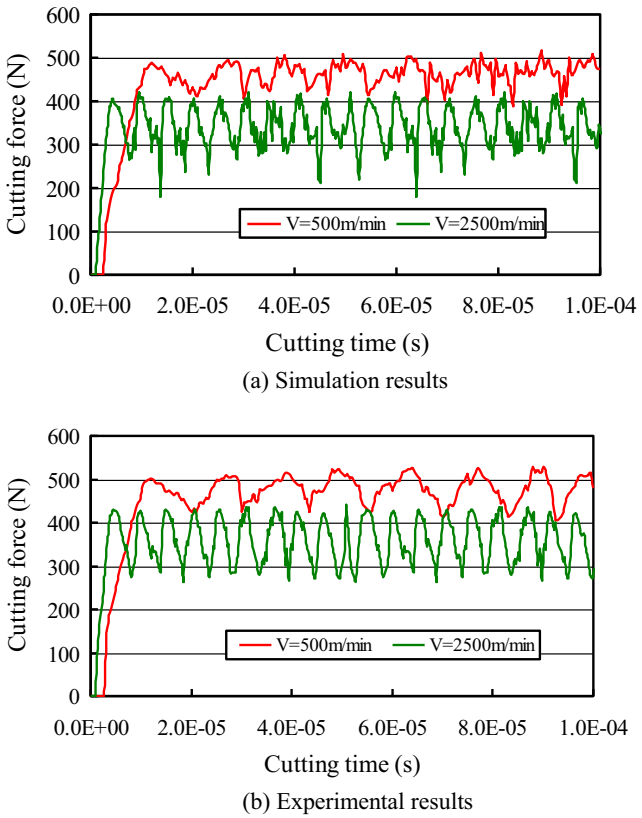

Fig. 9 Cutting forces under different cutting speeds. **a** Simulation results. **b** Experimental results

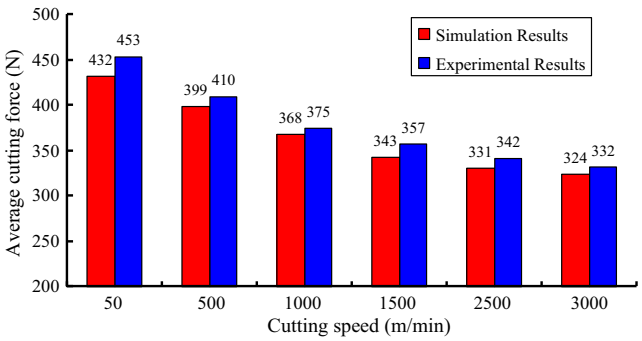

Fig. 10 Comparison of simulation and experimental average cutting forces under different cutting speeds

3.3 Analysis of cutting force

The simulation and experimental cutting forces under different cutting speeds are displayed in Fig. 9. The direction of the cutting force is parallel with Y-axis as shown in Figs. 2 and 4. It can be seen that the fluctuation occurs due to the cyclic generation of the shear bands in the serrated chips during machining. So, the fluctuant frequencies of cutting force approximate to the ones of chip serration. It can be seen from Fig. 9 that the simulation mean cutting force is 399 N (the experimental mean cutting force is 410 N) with a bandwidth of about 85 N for the cutting speed of 500 m/min. With regard to the cutting speed of 2,500 m/min, the simulation mean cutting force is 331 N (the experimental mean cutting force is 342 N) with a bandwidth of about 130 N. Both fluctuant frequency and amplitude of cutting force under 2,500 m/min are much larger than those under 500 m/min.

The variation of average cutting forces under different cutting speeds has also been analyzed as shown in Fig. 10. The simulation and experimental results of cutting forces are in good comparison. It can be deduced that the cutting force decreases with the cutting speed increasing. It can also be observed from Fig. 10 that the experimental cutting force is larger than that of the simulation results. The main reason lies in that the tool is regarded as sharp in the simulation process in which the cutting edge radius has not been considered. The decrease of cutting force under high cutting speed is a prominent advantage for high-speed machining, which has been widely used for the machining of thin-walled workpieces in aerospace industry.

Table 5 The researched JC fracture constants for Ti6Al4V

D_i	↓100 %	↓50 %	Original	↑50 %	↑100 %
D_1	−0.18	−0.135	−0.09	−0.045	0
D_2	0	0.125	0.25	0.375	0.5
D_3	−1.0	−0.75	−0.5	−0.25	0
D_4	0	0.007	0.014	0.021	0.028
D_5	0	1.935	3.87	5.805	7.74

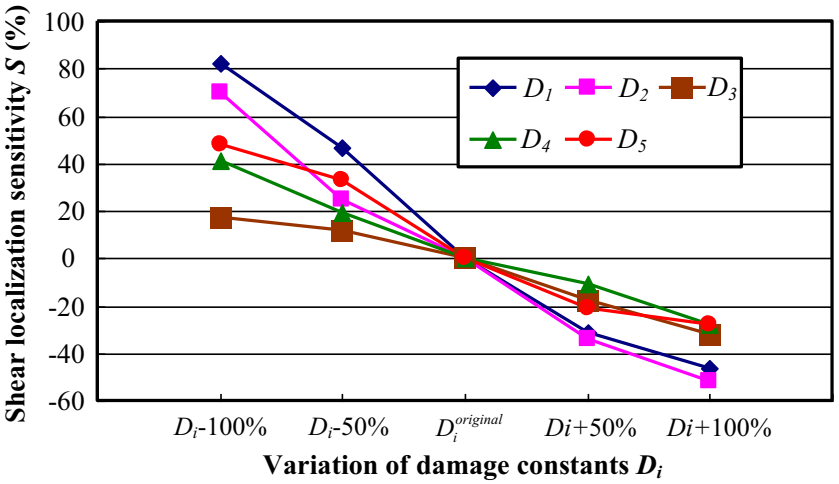

Fig. 11 Shear localization sensitivity of serrated chips to damage constants

4 Shear localization sensitivity of serrated chips to JC fracture constants

As mentioned in Section 2.3, the fracture constants D_i in Eq. (3) have direct influence on the fracture strain $\bar{\varepsilon}_f$, which will further determine the chip formation pattern in the cutting process. Considering the complexities of stress state and temperature distribution in the cutting shear zone, it is hard to analyze the influence mechanism of fracture constants on the chip formation mechanism through analytical method, which impels us to solve this problem based on finite element method. Through changing the five fracture constants individually, the serrated degrees of chips are quantitative analyzed, which means that the serrated degree is regarded as the reference parameter.

4.1 Determination of the range for five damage constants D_i

The original fracture constants of JC fracture model obtained by experiments [37] have been mentioned in Table 4. In order to investigate the influence of fracture constants on the chip formation in a wide range, the fracture constants are set in the range of decreasing 100 % to increasing 100 % on the basis of original values, with an interval of half of their original values. Table 5 shows the researched JC fracture constants for Ti6Al4V in this study.

4.2 Shear localization sensitivity of serrated chips to the fracture constants

The chip serrated degree is treated as the researched standard in this study. When the fracture constants are changed, the variation of serrated degrees compared to the original result can be analyzed quantitatively. This variation S is defined as the shear localization sensitivity as shown in Eq. (8).

$$S = \frac{G_s^{D_i} - G_s^{\text{original}}}{G_s^{\text{original}}} \times 100\ \% \tag{8}$$

where $G_s^{D_i}$ is the chip serrated degree under different fracture constants as shown in Table 5 based in Eq. (6), and G_s^{original} is the chip serrated degree under the original fracture constants based on Eq. (6). The cutting conditions are fixed at the cutting speed of 500 m/min and the uncut chip thickness of 0.1 mm in this section.

Figure 11 presents the shear localization sensitivity S under different JC fracture constants. It can be seen that when the JC fracture constants decrease, the shear localization sensitivity S is positive while it is negative when the JC fracture constants increase. The positive value of shear localization sensitivity means the increasing of chip serrated degree and vice versa, which can be attributed to the reason that the fracture strain $\bar{\varepsilon}_f$, has positive correlation with the five JC fracture constants as shown in Eq. (3). It is shown in Fig. 11 that the effects of JC fracture constants D_1 and D_2 on the shear localization of serrated chips are more conspicuous, no matter promotion or suppression. The effect of parameter D_3 on shear localization is the least apparent, and the parameters D_4 and D_5 fall in between.

When a certain one of JC fracture constants is zero, for example the parameter D_5 is zero, the individual effect of temperature on the shear localization of serrated chip can be obtained. In this way, the individual effects of the initial failure strain, the stress triaxiality, the strain rate, and the temperature on the shear localization can be deduced as shown in Fig. 12. It can be seen that when the parameter D_1 or D_3 is zero, the shear localization is suppressed while the shear localization is promoted when the other three parameters are zero.

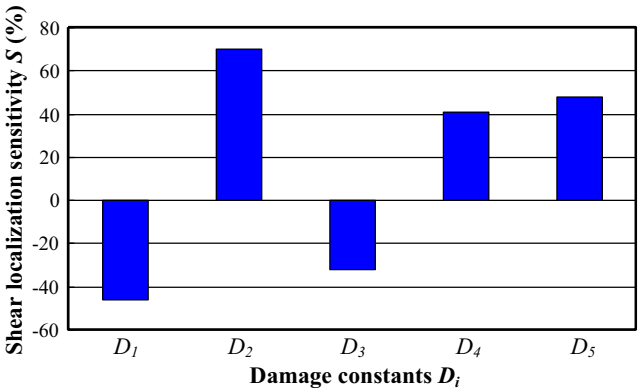

Fig. 12 Shear localization sensitivity of serrated chips when the respective fracture constant D_i is zero

Furthermore, the shear localization sensitivity is the largest when the parameter D_2 is zero, which illustrates the great influence of stress triaxiality on the chip serration. The analysis of stress state in the cutting shear zone has vital importance on the understanding of chip formation mechanism.

Figure 13a–e shows the distribution of damage variable D (scalar stiffness degradation, SDEG) of serrated chips when each JC fracture constant is zero, respectively. Figure 13f shows the distribution of damage variable D under the original JC fracture constants. It can be seen that the value of SDEG is much less than the failure value (i.e., when damage variable D equals to 1) when the parameter D_1 or D_3 is zero, so the serrated degree of chip is smaller than that of the original JC fracture constants. In contrast, the value of SDEG in the primary shear zone approaches the failure value which results in the aggravation of chip serration when the parameter D_2 or D_5 is zero. It can be seen from Fig. 13b, e that some adjacent segments nearly separate from each other completely, which are illustrated by the red marks in the figures. Moreover, the bending of the chip is severer due to the degradation of joint strength between adjacent segments.

5 Conclusions

The simulation of cutting process can help to get deeper insights into the cutting mechanism. There are two main parts included in this paper. The first one is to carry out the high-speed cutting process of Ti6Al4V with the aid of both simulations and experiments, which gives good accordance covering the chip morphology and cutting force in the two methods. The second one is to investigate the influence of JC fracture constants on the chip formation based on the finite element method, which is the main innovative work conducted in this

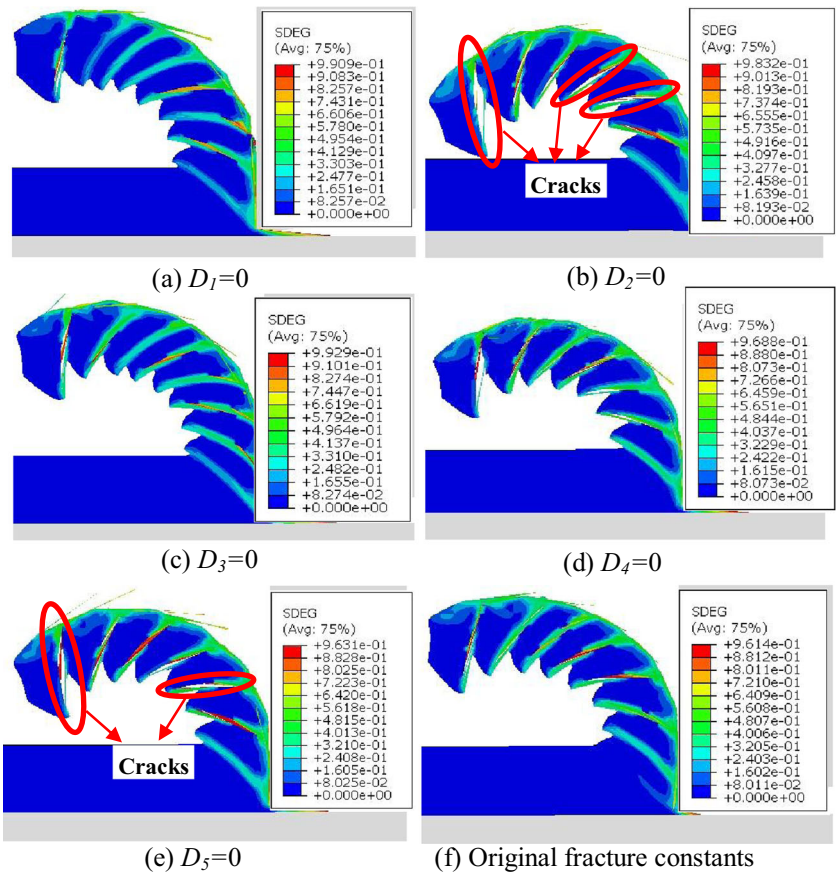

Fig. 13 Distribution of damage variable D (scalar stiffness degradation, SDEG) under different JC fracture constants

study. Some interesting results have been concluded as follows:

1. Both the simulation and experimental results show that with the cutting speed increasing, the chip serrated degree increases until it tends to one when the chip morphology becomes unit or fragmented. For the orthogonal cutting process of Ti6Al4V, the cutting speed turning point of chip morphology from serrated to unit is about 2,500 m/min.
2. The research shows that the serrated frequency of chips has positive correlation with the cutting speed. When the chip morphology becomes unit, the serrated frequency could not be used to describe the geometric characteristic of chips.
3. With the cutting speed increasing, the mean value of the cutting forces decreases. When the chip morphology evolves from serrated to unit ones under ultra high cutting speed, both the fluctuant frequency and fluctuant amplitudes of the cutting forces increase sharply due to the occurrence of ductile to brittle fracture transition at the chip deformation zone.
4. The shear localization sensitivity is firstly proposed to describe the influence of JC fracture constants on the chip formation process. When the JC fracture constants decrease, the shear localization sensitivity is positive while it is negative when the JC fracture constants increase.
5. The research indicates that the influences of initial failure strain D_1 and exponential factor of stress triaxiality D_2 on the chip formation process are more conspicuous than those of the rest three ones.
6. Through studying the individual effects of the initial failure strain, the stress triaxiality, the strain rate, and the temperature on the shear localization of chips, the conclusion can be drawn that the decreased ranking of effect degree for these variables is the stress triaxiality, the temperature, the initial failure strain, and the strain rate.

Acknowledgments This work was supported by grants from Tai Shan Scholar Foundation. The authors would like to acknowledge the financial support from the National Natural Science Foundation of China (51375272, U1201245) and the Major Science and Technology Program of High-end CNC Machine Tools and Basic Manufacturing Equipment (2014ZX04012-014).

References

1. Ezugwu EO, Wang ZM (1997) Titanium alloys and their machinability—a review. J Mater Process Technol 68:262–274
2. Niu W, Bermingham MJ, Baburamani PS, Palanisamy S, Dargusch MS, Turk S, Grigson B, Sharp PK (2013) The effect of cutting speed and heat treatment on the fatigue life of grade 5 and grade 23 Ti-6Al-4V alloys. Mater Des 46:640–644
3. Arrazola PJ, Garay A, Iriarte LM, Armendia M, Marya S, Maître FL (2009) J Mater Process Technol 209:2223–2230
4. Armendia M, Garay A, Iriarte LM, Arrazola PJ (2010) Comparison of the machinabilities of Ti6Al4V and TIMETAL® 54 M using uncoated WC-Co tools. J Mater Process Technol 210:197–203
5. Sutter G, List G (2013) Very high speed cutting of Ti-6Al-4V titanium alloy-change in morphology and mechanism of chip formation. Int J Mach Tools Manuf 66:37–43
6. Molinari A, Soldani X, Miguélez MH (2013) Adiabatic shear banding and scaling laws in chip formation with application to cutting of Ti-6Al-4V. J Mech Phys Solids 61:2331–2359
7. Ginting A, Nouari M (2009) Surface integrity of dry machined titanium alloys. Int J Mach Tool Manuf 49:325–332
8. Bhaumik SK, Divakar C, Singh AK (1995) Machining Ti-6Al-4V alloy with a wBN-cBN composite tool. Mater Des 16:221–226
9. Bakkal M, Shih AJ, Scattergood RO (2004) Chip formation, cutting forces, and tool wear in turning of Zr-based bulk metallic glass. Int J Mach Tool Manuf 44:915–925
10. Sutter G (2005) Chip geometries during high-speed machining for orthogonal cutting condition. Int J Mach Tool Manuf 45:719–726
11. Joshi SS, Ramakrishnan N, Ramakrishnan P (2001) Micro-structural analysis of chip formation during orthogonal machining of Al/SiCp composites. J Eng Mater Technol 123:315–321
12. Shaw MC, Vyas A (1993) Chip formation in the machining of hardened steel. CIRP Ann Manuf Technnol 42:29–33
13. Nakayama K, Arai M, Kada T (1988) Machining characteristics of hard materials. CIRP Ann Manuf Technnol 37:89–92
14. Elbestawi MA, Srivastava AK, El-Wardany TI (1996) A model for chip formation during machining of hardened steel. CIRP Ann Manuf Technnol 45:71–76
15. Özel T (2009) Computational modelling of 3D turning: influence of edge micro-geometry on forces, stresses, friction and tool wear in PcBN tooling. J Mater Process Technol 209:5167–5177
16. Pramanik A, Zhang LC, Arsecularatne JA (2007) An FEM investigation into the behavior of metal matrix composites: tool-particle interaction during orthogonal cutting. Int J Mach Tool Manuf 47:1497–1506
17. Mabrouki T, Girardin F, Asad M, Rigal JF (2008) Numerical and experimental study of dry cutting for an aeronautic aluminium alloy (A2024-T351). Int J Mach Tool Manuf 48:1187–1197
18. Baker M (2005) Finite element investigation of the flow stress dependence of chip formation. J Mater Process Technol 167:1–13
19. Davim JP, Maranhão C (2009) A study of plastic strain and plastic strain rate in machining of steel AISI 1045 using FEM analysis. Mater Des 30:160–165
20. Zahedi SA, Demiral M, Roy A, Silberschmidt VV (2013) FE/SPH modelling of orthogonal micro-machining of f.c.c. single crystal. Comput Mater Sci 78:104–109
21. Calamaz M, Coupard D, Girot F (2008) A new material model for 2D numerical simulation of serrated chip formation when machining titanium alloy Ti-6Al-4V. Int J Mach Tool Manuf 48:275–288
22. Rosa PAR, Martins PAF, Atkins AG (2007) Revisiting the fundamentals of metal cutting by means of finite elements and ductile fracture mechanics. Int J Mach Tool Manuf 47:607–617
23. Zhang YC, Mabrouki T, Nelias D, Gong YD (2011) FE-model for titanium alloy (Ti-6Al-4V) cutting based on the identification of limiting shear stress at tool-chip interface. Int J Mater Form 4:11–23
24. Chen G, Ren CZ, Yang XY, Jin XM, Guo T (2011) Finite element simulation of high-speed machining of titanium alloy (Ti-6Al-4V) based on ductile failure model. Int J Adv Manuf Technol 56:1027–1038
25. Childs THC (1998) Material property needs in modeling metal machining. Mach Sci Technol 2:303–316
26. Astakhov VP, Outeiro JC (2005) Modeling of the contact stress distribution at the tool-chip interface. Mach Sci Technol 9:85–99

27. Guo YB, Yen DW (2004) A FEM study on mechanisms of discontinuous chip formation in hard machining. J Mater Process Tech 155–156:1350–1356
28. Özel T, Zeren E (2007) Finite element modeling the influence of edge roundness on the stress and temperature fields induced by high-speed machining. Int J Adv Manuf Technol 35: 255–267
29. Ambati R, Yuan H (2011) FEM mesh-dependence in cutting process simulations. Int J Adv Manuf Tech 53:313–323
30. Umbrello D (2008) Finite element simulation of conventional and high speed machining of Ti6Al4V alloy. J Mater Process Technol 196:79–87
31. Hosseini E, Kazeminezhad M (2011) Implementation of a constitutive model in finite element method for intense deformation. Mater Des 32:487–494
32. Mabrouki T, Rigal JF (2006) A contribution to a qualitative understanding of thermo-mechanical effects during chip formation in hard turning. J Mater Process Technol 176:214–221
33. Menezes PL, Avdeev IV, Lovell MR, Higgs CF III (2014) An explicit finite element model to study the influence of rake angle and friction during orthogonal metal cutting. Int J Adv Manuf Technol. doi:10.1007/s00170-014-5877-5
34. Deng WJ, Xia W, Tang Y (2009) Finite element simulation for burr formation near the exit of orthogonal cutting. Int J Adv Manuf Tech 43:1035–1045
35. Abaqus Inc (2006) Analysis user's manual. Version 6.6, USA
36. Johnson GR, Cook WH (1983) A constitutive model and data for metals subjected to large strains, high strain rates and high temperatures. In: Proceedings of the seventh international symposium on ballistics. Hague, Netherlands. 541–547
37. Johnson GR, Holmquist TJ (1989) Test data and computational strengthen and fracture model constants for 23 materials subjected to large strain, high-strain rates, and high temperatures. Los Alamos National laboratory, LA-11463-MS
38. Johnson GR, Cook WH (1985) Fracture characteristics of three metals subjected to various strains, strain rates, temperatures and pressures. Eng Fract Mech 21:31–48
39. Hillerborg A, Modéer M, Petersson PE (1976) Analysis of crack formation and crack growth in concrete by means of fracture mechanics and finite elements. Cem Concr Res 6:773–781
40. Schulz H, Abele E, Sahm A (2001) Material aspects of chip formation in HSC machining. CIRP Ann Manuf Technnol 50:45–48
41. Belhadi S, Mabrouki T, Rigal JF, Boulanouar L (2005) Experimental and numerical study of chip formation during straight turning of hardened AISI 4340 steel. Proc Inst Mech Eng Part B: J Eng Manuf 219:515–524
42. Liu ZQ, Su GS (2012) Characteristics of chip evolution with elevating cutting speed from low to very high. Int J Mach Tool Manuf 54–55:82–85
43. Molinari A, Musquar C, Sutter G (2002) Adiabatic shear banding in high speed machining of Ti-6Al-4V: experiments and modeling. Int J Plast 18:443–459